

Tension Stiffening Behavior of GFRP-Reinforced Concrete

by H. Sooriyaarachchi, K. Pilakoutas, and E. Byars

Synopsis: This paper presents an experimental study into the structural response of Glass Fiber Reinforced Polymers Reinforced Concrete (GFRP-RC) tension members. The influence of concrete strength, reinforcement ratio and bar diameter on tension stiffening is investigated by testing elements in direct tension. Using bars specially manufactured with internal strain gauges, typical strain patterns occurring between cracks during direct tension tests were measured and bond stresses derived, thereby obtaining the information for modeling tension stiffening behavior of GFRP-RC. An increase in the tension stiffening behavior with decrease in reinforcement ratio and increase in concrete strength was observed. No appreciable change in tension stiffening was recorded with changes in bar diameter at constant reinforcement ratio. This paper also discusses the limitations that may be encountered in modifying current models to represent the tension stiffening effect of GFRP-RC.

Keywords: bar diameter; bond (concrete to reinforcement); GFRP-RC; reinforcement ratio; strain patterns; tension stiffening

976 Sooriyaarachchi et al.

Harsha Sooriyaarachchi is a research scholar reading for his PhD in the Department of Civil and Structural Engineering University of Sheffield, UK. He received his BSc.Eng from the University of Moratuwa, Sri Lanka and his MEng from the University of Tokyo, Japan. His research interest includes bond, structural behavior of concrete and repair of concrete structures.

ACI Member Kypros Pilakoutas PhD, DSc, is a Professor of Construction Innovation Department of Civil and Structural Engineering, University of Sheffield, Sheffield, UK. He is the convener of the Federation Internationale du Beton (fib) Task Group (TG) 9.3 FRP (Fibre Reinforced Polymer) Reinforcement for Concrete Structures and a member of fib TG 4.2 on bond models.

Ewan Byars PhD, Head of the Concrete Materials Research Unit (CMRU) in the Department of Civil and Structural Engineering, University of Sheffield, UK has concrete research interests in new materials, durability and binder technology. He sits on ACI Committee C666 (Recycled Materials) and Federation Internationale du Beton (fib) Task Group (TG) 9.3 FRP (Fibre Reinforced Polymer) Reinforcement for Concrete Structures.

INTRODUCTION

General

The relatively low stiffness of GFRP internal reinforcement compared with steel reinforcement often makes the limit of deflection or crack width at service loads the governing criterion for design. This makes prediction of deflections, particularly at service loads, more important for the design of GFRP-RC than for steel reinforced structures. The contribution of concrete in the tension zone can be a controlling factor in determining deflections and cracking and until now no work has been reported on GFRP-RC tensile behavior.

There are several design recommendations and guidelines for designing FRP reinforced concrete members including the JSCE 1997, EUROCRETE 1997 and ACI 440-1R-03. The ACI 440-1R-03 design equations are based on the ACI 318-05 code for design of steel RC and are the most widely used set of recommendations. However, predictions of serviceability limit state performance of FRP-RC members with these equations have been found to be unconservative especially at low reinforcement ratios. Toutanji et al. 2003 summarizes the results of Yost 1983, Masmoudi et al. 1998 and Benmokarane et al. 1995 and illustrated the difference between measured and predicted deflections (based on Branson's formulae used in ACI) of FRP reinforced concrete beams at service loads (50% maximum load). They concluded that there is an increase in inaccuracy at low reinforcement ratios. Abdalla 2002 examined the ACI 440 modification to Branson's equation and found that it too was not adequate for predicting deflections at low reinforcement ratios. The accuracy of these deflection predictions largely depends on how the effective moment of inertia (I_e) of partially cracked sections is determined. The effective moment of inertia accounts for two different phenomena: 1) variation of stiffness along the member and 2) effect of concrete tension stiffening. Due to the limitations of these equations in estimating deflection of FRP, various

researchers (Faza et al. 1992, Alsayed et al. 2000, and Abdalla 2002) came up with different modifications for calculating I_e of partially cracked sections. However it is the authors' belief that a better understanding of tension stiffening behavior is essential to develop more accurate equations for predicting the performance of FRP in concrete.

The apparent ability of concrete to carry stress in the tensile strain region following tensile cracking is known as tension stiffening and is primarily a result of bond between concrete and reinforcement, as well as the relative stiffness of concrete and reinforcements. An experimental determination of the tension stiffening effect of concrete using FRP as internal reinforcement has never been attempted.

Significance of the study

This paper reports experimental results and concepts that could lead to modeling tension stiffening effects by using a direct tension test. Although simple RC members in pure tension are unlikely to exist in practice, it is felt that, experimentally at least, they provide the ideal platform to evaluate the influence of various parameters on the tension stiffening behavior. This study examines the influence of different reinforcement ratios, concrete compressive strength and bar diameter on the tension stiffening behavior. In addition strain gauged bars are used to examine the strain pattern occurring during direct tension test and bond stress variation between cracks. Finally, two existing equations have been modified and the ability of these modified equations to predict the tension stiffening effect of GFRP-RC is discussed.

EXPERIMENTAL PROGRAM

Testing GFRP reinforcing bars in tension is not trivial since the bars need to be gripped without crushing and damage. In this experimental work the ends of GFRP bars were bonded in hollow threaded steel bars to avoid crushing at the pull-ends. Both bare bar and reinforced concrete tensile specimens were tested using the testing arrangement shown in Fig. 1 and 2 with the actuator and bar-holding device reacting against a rigid steel frame. Fig. 2 illustrates the measuring arrangement used on one end of the GFRP RC tension specimen. Measurements of concrete strain (predominantly due to cracking of concrete) were done using three LVDT's equally spaced at 120° around the centre line of the concrete specimen. The LVDT's were attached to one end of the concrete specimen and connected to fixed points of the other end using a 0.2 mm diameter special light weight wire. Bond slip at each end was measured by using a collar, having three small LVDT's equally spaced at 120° , attached on the bar as shown in Fig. 2. A 50 mm debonded length was maintained on either side of all tensile specimens where transducers were fixed to avoid local concrete tensile failure.

When determining the composite stress-strain behavior of the RC element in tension, it is necessary that displacements are measured with reference to the movements of the bar from one end of the specimen to the other end. Considering the measuring arrangement used in this experimental work, the total elongation of the test specimen is equal to the sum of the end slips TD_{slip} plus the total concrete displacement $TD_{concrete}$.

978 Sooriyaarachchi et al.

Therefore, the composite strain ($\epsilon_{composite}$) of the reinforced concrete element with composite length, l , at given applied load, P , can be determined as shown below Eq. (1).

$$\epsilon_{composite} = \frac{(TD_{slip})_{L\&R} + TD_{concrete} - P/(A_f E_f) \times DL_{L\&R}}{l} \dots\dots\dots (1)$$

Where $DL_{L\&R}$ refers to the sum of de-bonded length at both ends (see Figure 2) and any additional length requirements to fix transducers measuring slip TD_{slip} to the reinforcement bar. $(TD_{slip})_{L\&R}$ refers to the sum of average end slip at both ends.

A distinct advantage of this measuring arrangement is that it minimizes any errors that can be induced by global changes to the specimen while loading, as measurements are done locally. All specimens were loaded with displacement control to avoid sudden movements during concrete cracking.

For the purpose of measuring the strain profile along the bar, strain gauges are normally attached on the bar surface at close centers in the vicinity of the cracked regions. The problem with a series of strain gauges on the surface is that their presence interferes with bond development, and, hence, can adversely influence the test results. To avoid such problems in these experiments strain gauges were placed at 50mm centers in the centre of the bars. Conventional foil wire strain gauges were glued on a bar cut longitudinally in half. On the other half a groove 4 mm wide and 3mm deep was cut to accommodate the gauges and wiring. After that the two halves were glued together to form one round bar Fig. 3. Because of the limitations of the area required to work all these details, strain gauging was done only on 19 mm bar.

In this experimental work two concrete grades and two GFRP bar diameters were used for specimens with square concrete cross-sections of 100, 150, and 200 mm. After casting all the tensile specimens the concrete control specimens were cured at 20°C 100% relative humidity. The curing was done carefully and consistently for all the specimens to control the effects of shrinkage and plastic shrinkage cracking on the tension stiffening behavior. Table 1 gives details of the test specimens that form the discussion of this paper whilst Table 2 gives the important material properties of concrete and GFRP bar used in this experimental program.

TEST RESULTS

Bond behavior between cracks

Typical strain distributions along the length of the bar while cracking is taking place are shown in Fig. 4 for specimen C50/19/200N. This specimen had three cracks induced at equal distance by cutting 25 mm deep notches all round the section using a diamond saw. Results are plotted for three different loading conditions: i) the strain distribution just before the first crack at 37 kN, Fig. 4(a) ii) just before and after the second crack at 43 kN, Fig. 4(b) and iii) just before and after third crack at 53kN tensile load, Fig. 4(c) . The strain patterns make it clear that substantial composite action between cracks prevails until the end of the crack development stage. However, by the time the third crack is

occur during cracking with large increments of strain for relatively low stress increments, Fig. 5 represents, on the other hand, the post cracking response with relatively low concrete contribution to the tensile load bearing capacity.

Influence of reinforcement ratio— It is important to understand how the area of concrete around the bar contributes to the tension stiffening effect. Fig. 8 compares the tension stiffening effect of different reinforcement ratios tested in this study. As the experimental work involved testing two grades of concrete, the results are plotted in separate graphs: Fig. 8(a) shows grade 50 concrete whilst Fig. 8(b) shows grade 90 concrete. It is clear from the figures that tension stiffening increases with a decrease in reinforcement ratio. However, it is not clear whether the effect is directly proportional to the decrease in reinforcement ratio.

Influence of concrete strength— Concrete strength can influence the tension stiffening behavior in two different ways. Firstly, high strength concrete requires higher loads to crack the specimens. In addition, better bond between concrete and reinforcement allows stresses to be transferred more effectively between the bar and concrete making the average stress contribution of concrete higher. Fig. 9 illustrates this effect by comparing different concrete strengths at constant reinforcement ratio.

Influence of bar size on tension stiffening behavior— Bar size is one other factor that might influence tension stiffening. However, in this experimental study no significant influence on tension stiffening is recorded for different bar sizes when results of same reinforcement ratio are compared as shown in Fig. 10.

Concrete contribution

When modeling using the smeared crack approach, the tension stiffening effect is included in the average stress strain behavior of concrete in tension. The average stress-strain relationships of concrete derived from the direct tension tests of Fig. 9(a) are shown in Fig. 11. Average concrete tensile stress ($\sigma_{t,concrete}$) is derived by deducting the average force contribution of the reinforcement bar from the overall response of the specimen and averaging the remaining force over the concrete cross section (A_c) by assuming a uniform stress distribution of concrete across and along the test specimen Eq.(3).

$$\sigma_{t,concrete} = \frac{\sigma_{Rebar} \times A_f - \epsilon_{composite} \times A_f \times E_f}{A_c} \dots\dots\dots(3)$$

Where σ_{Rebar} is the reinforcement stress at the crack section.

PREDICTION OF TENSION STIFFENING

There are two main models that deal with tension stiffening behavior of steel reinforcement which can be adopted with modification for GFRP: 1) The ACI model as given in (ACI 224.2R-86) which takes into account the average effective cross sectional

area, A_e , Eq. (4); 2) The CEB model (CEB-FIP Model code) which introduces a method of calculating the average strain, ϵ_m , of a member for a given loading after concrete cracking Eq. (8).

The ACI-224 approach is analogous to the approach adopted for the effective moment of inertia, I_e , in ACI-318 (see Eq. (4) and Eq. (5)). The ACI-318 equation has been adopted and modified by ACI committee 440 as shown in Eq. (6) for the use of FRP reinforcement. The modification factor β_d used by ACI 440 to account for the low bond stress of FRP is applied here to Eq. (4) in deriving Eq. (7) for this analysis. The CEB model shown in Eq. (8) is more phenomenological in the sense that it considers a decreasing trend for tension stiffening with increasing strain after cracking.

ACI 224.2R-92
$$A_e = \left[\frac{P_{cr}}{P_a} \right]^3 A_g + \left[1 - \left(\frac{P_{cr}}{P_a} \right)^3 \right] A_{cr} \dots\dots\dots(4)$$

ACI-318
$$I_e = \left[\frac{M_{cr}}{M_a} \right]^3 I_g + \left[1 - \left(\frac{M_{cr}}{M_a} \right)^3 \right] I_{cr} \dots\dots\dots(5)$$

where
$$I_g = \frac{bh^3}{12}, \quad I_{cr} = \frac{bd^3}{3} k^3 + n_f A_f d^2 (1 - k^2)$$

$$k = \sqrt{2n_f \rho_f + (\rho_f n_f)^2} - \rho_f n_f$$

$$n_f = \frac{E_f}{E_c}, \quad \rho_f = \frac{A_f}{A_g}, \quad E_c = 4560 \sqrt{f'_c}$$

ACI- 440
$$I_e = \left[\frac{M_{cr}}{M_a} \right]^3 \beta_d I_g + \left[1 - \left(\frac{M_{cr}}{M_a} \right)^3 \right] I_{cr} \dots\dots\dots(6)$$

Adjusted for this Study
$$A_e = \left[\frac{P_{cr}}{P_a} \right]^3 \beta_d A_g + \left[1 - \left(\frac{P_{cr}}{P_a} \right)^3 \right] A_{cr} \dots\dots\dots(7)$$

where
$$\beta_d = \alpha_b \left[\frac{E_f}{E_s} + 1 \right] \quad \alpha_b = 0.5,$$

CEB
$$\epsilon_m = \epsilon_f \left[1 - K \left(\frac{f_{scr}}{f_f} \right)^2 \right] \dots\dots\dots(8)$$

where
$$f_{scr} = \frac{P_{cr}}{A_f} = f'_t \left(\frac{1}{\rho} - 1 + n_f \right), \quad f'_t = 0.6 \sqrt{f'_c}$$

K=accounts for the bond and considered as 0.5 in the calculation

Predictions of the concrete contribution to tension stiffening using the CEB model (calculated according to Eq. (8)) and the modified ACI model (calculated according to

982 Sooriyaarachchi et al.

Eq. (7)) for grade 50 concrete and the corresponding test results (C50/13/100, C50/13/150 & C50/13/200) are shown in Fig. 12. It is clear from this analysis that even the modified ACI-224 model (Eq. (7)) grossly overestimates the tension stiffening effect of GFRP RC. It is also noted that with the increase of reinforcement ratio the modified ACI-224 equation (Eq. (7)) tends to make more sense. The trend observed can be linked with the underestimation in deflections for flexural elements with low reinforcement ratios. Compared to ACI, the CEB model (with the appropriate modification factor for bond) is more accurate in predicting tension stiffening behavior, although it still is unconservative.

CONCLUSIONS

Concrete strength and reinforcement ratio were found to have an influence on tension stiffening behavior. There is no significant influence on tension stiffening behavior due to changes in bar diameter. From the results of strain distribution it is clear that there is loss of full composite action at higher loads when no more cracks develop. It is further seen that bond degradation occurs near cracks at an early stage and that this degradation migrates away from the crack with increasing load. After evaluating various models it has been found that the ACI-224 method grossly overestimates the tension stiffening effect of concrete particularly at low reinforcement ratios. Given the similarities of the equation to the equation for calculating the moment of inertia in the deflection calculations, it is reasonable to conclude that the ACI 440 equation for predicting deflections will overestimate the tension stiffening effects of concrete particularly at low reinforcement ratios. The CEB model has a better approach in calculating tension stiffening, but it still overestimates the experimental results.

More fundamental work is currently being done on the bond behavior and strain behavior of GFRP RC and a better understanding of these aspects can form a basis for accurate predictions of tension stiffening effect of concrete. Further research is also required to incorporate the actual tension stiffening effects of concrete in deflection and crack width calculations.

NOTATION

P_{cr}	Axial load at which cracking occurs	h	Height of rectangular section
	N		mm
P_a	Load carried by reinforcements	E_f	Modulus of elasticity of FRP
	N		N
			mm^2
A_e	Effective cross sectional area	E_c	Modulus of elasticity concrete
	mm^2		N
			mm^2
A_g	Gross cross sectional area	E_s	Modulus of elasticity of steel
	mm^2		N
			mm^2
A_{cr}	Cracked cross sectional area	A_f	Area of FRP reinforcement
	mm^2		mm^2
I_e	Effective second moment of inertia	A_g	Gross area of the section
	mm^4		mm^2
I_g	Gross second moment of inertia	f'_c	Concrete compressive strength
			N

I_{cr}	mm^4 Cracked second moment of inertia mm^4	ε_m	mm^{-2} Average strain of RC element
M_a	Applied moment Nmm	ε_f	Strain of FRP reinforcement
M_{cr}	Cracking moment of the section Nmm	f_f	Stress in reinforcement $N\ mm^{-2}$
b	Breadth of a rectangular section mm	f'_t	Tensile strength of concrete $N\ mm^{-2}$
d	Effective depth of concrete section mm	f_{scr}	Rebar stress after crack $N\ mm^{-2}$

REFERENCES

- Abdalla, H.A., 2003, "Evaluation of Deflection in Concrete Members Reinforced with Fiber Reinforced Polymer (FRP) bars", *Composite Structures*, Vol. 56, pp. 63-71.
- ACI Committee 224, 1986, "Cracking of Concrete Members in Direct Tension (ACI 224.2R-86)," American Concrete Institute, Detroit, 11 pp.
- ACI Committee 440, 2003, "Guide for the Design and Construction of Concrete Reinforced with FRP Bars (ACI 440.1R-03)," American Concrete Institute, Farmington Hill, Michigan, 42 pp.
- ACI Committee 318, 2005, "Building Code Requirements for Structural Concrete (ACI 318-05) and Commentary (ACI 318R-05)", American Concrete Institute, Farmington Hills, Michigan, pp. 111-115.
- Alsaied, S.H.; Al-Saloum, Y.A. and Almusallam, T.H., 2000, "Performance of glass fibre reinforced plastic bars as a reinforcing material for concrete structures" , *Composites: Part B: Engineering*, Vol. 31, pp. 555-567.
- CEB-FIP, "CEB-FIP Model Code for Concrete Structures," *Comite Euro-International du Beton and Federation Internale de la Precontrainte*, CEB, 1978, 348 pp.
- Eurocrete Project., 1997, "The development of non-ferrous reinforcement for concrete structures- final report," Prepared by *Euro-Project (LTTC) ltd*, 109 pp.
- Hsu, T.T.C., 1988, "Softened Truss Model Theory for Shear and Torsion," *American Concrete Institute Structural Journal*, Vol. 85, (6), pp. 624-634.
- JSCE, 1997, "Recommendation for design and construction of concrete structures using continuous fiber reinforcing materials", *Japan Society of Civil Engineers*, October 1997.
- Toutnaji, H. and Deng, Y., 2003, "Deflection and Crack Width Prediction of Concrete Beams Reinforced with Glass FRP Rods," *Construction and Building Materials*, Vol. 17, pp. 69-74.
- Vecchio, F.J., Collins, M.P., March (1986): "The modified compression field theory for reinforced concrete elements subjected to shear", *American Concrete Institutel Journal*, Vol. 83, No. 2., pp. 219- 231.

Table 1— Details of the test specimens

Specimen	Concrete Strength (MPa)	Bar Diameter D (mm)	Dimensions $b \times d \times l$ (mm)	Reinforcement Ratio ρ %
C50/13/100	52	12.7	100×100×1500	1.26
C50/13/150	52	12.7	150×150×1500	0.56
C50/13/200	52	12.7	200×200×1500	0.32
C90/13/100	91	12.7	100×100×1500	1.26
C90/13/150	91	12.7	150×150×1500	0.56
C50/19/150	52	19.1	150×150×1300	1.27
C50/19/200	52	19.1	200×200×1300	0.72
C90/19/150	91	19.1	150×150×1300	1.27
C90/19/200	91	19.1	200×200×1300	0.72
C50/19/200N	52	19.1	200×200×1300	0.72

Table 2— Material properties

PROPERTY	GFRP BAR		CONCRETE STRENGTH	
	13 mm bar	19 mm bar	Grade 50	Grade 90
Strength (MPa)	792	715	52.0	91.0
Stiffness (GPa)	42.9	41.9	36.2	48.3
Splitting tensile strength (MPa)			2.9	5.2



Figure 1— Testing arrangement of horizontally loaded tension member

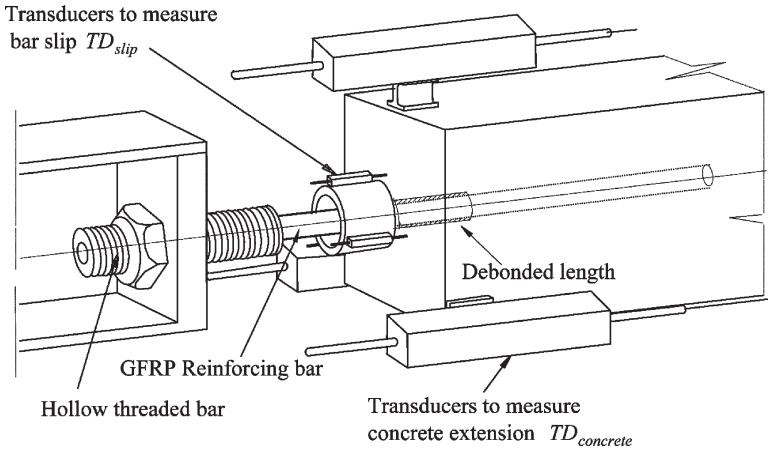


Figure 2— Measuring arrangement for measuring average strain of the specimen

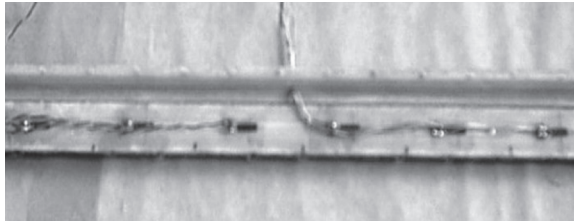


Figure 3—Two halves of strain gauged bar just before Gluing

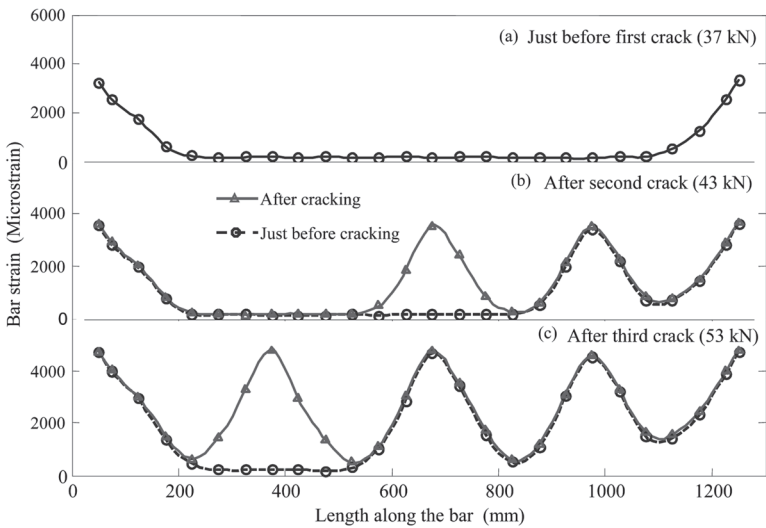


Figure 4— Shows the strain pattern along the during crack development stage

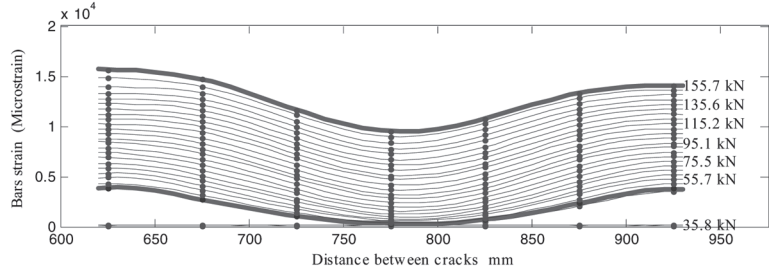


Figure 5— Post cracking strain pattern between cracks

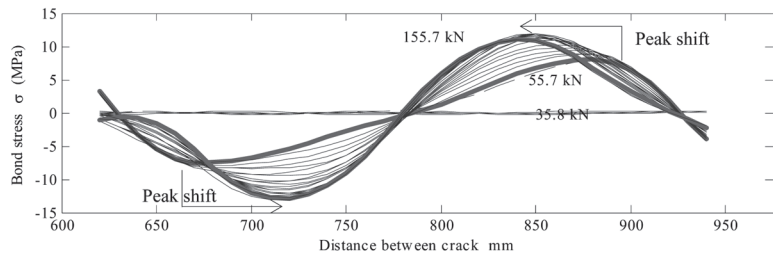


Figure 6— Bond stress between cracks

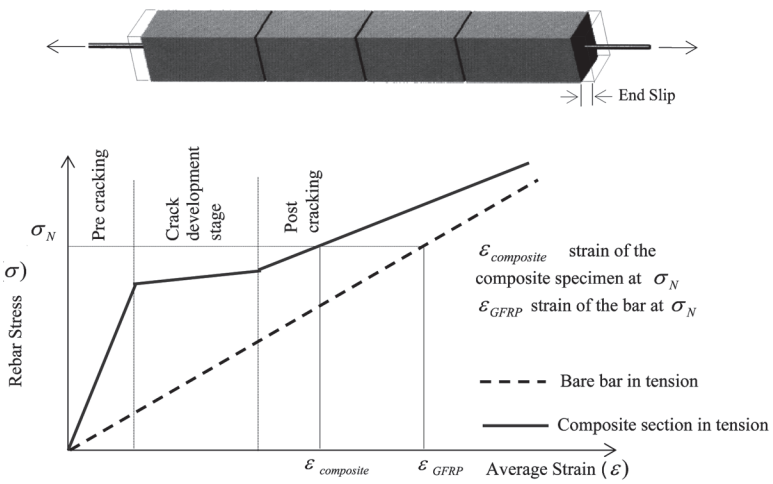


Figure 7— Overall performance of direct tensile test interpreted in terms of stress strain behavior of reinforcement.

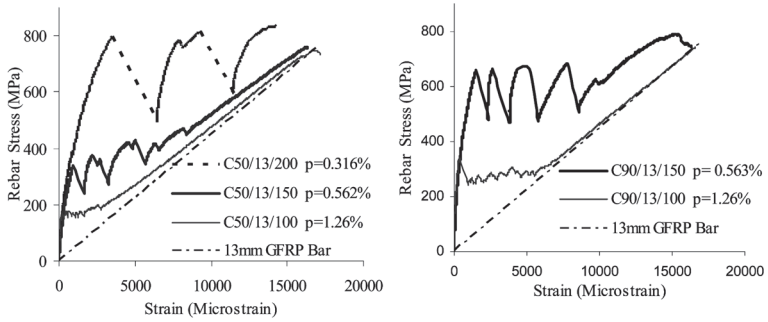


Figure 8— Influence of reinforcement ratio on the tension stiffening (a) C 50 (b) C90

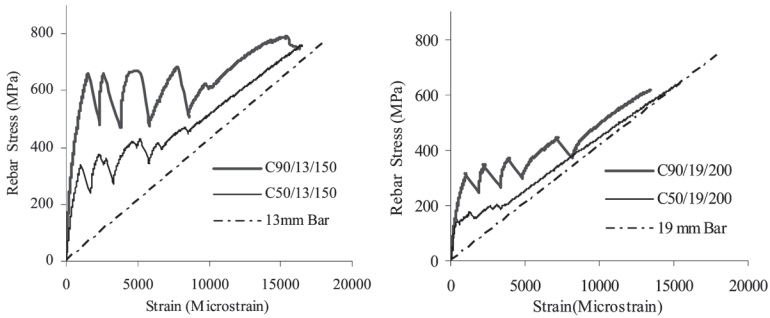


Figure 9— Influence of concrete strength on tension stiffening (a) 13 mm (b) 19 mm bar

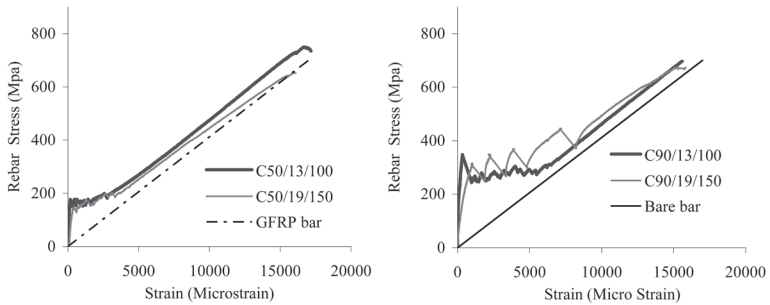


Figure 10— Influence of bar diameter on tension stiffening (a) C50 (b) C90 concrete ($\rho = 1.26\%$)

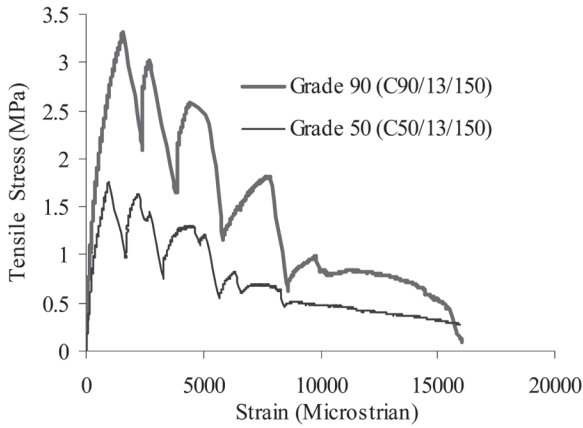


Figure 11— The average stress-strain relationship of concrete

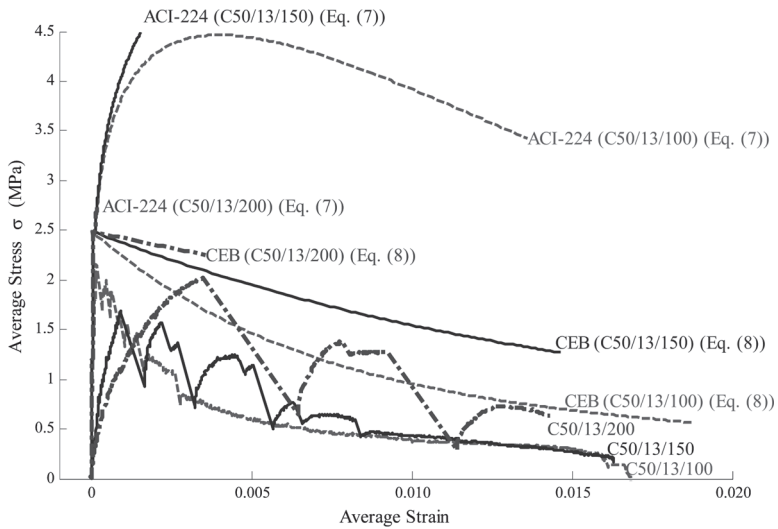


Figure 12— Comparison of test results with estimates of ACI (Eq. (7)) and CEB (Eq. (8)) models

